Anatomy assisted MAP-EM PET image reconstruction incorporating joint entropies of wavelet subband image pairs

Jing Tang and Arman Rahmim

***Abstract*–A promising approach in PET image reconstruction is to incorporate high resolution anatomical information (measured from MR or CT) taking the anato-functional mutual information (MI) or its joint entropy (JE) as the prior. The MI or JE of the images only classify voxels based on intensity, while neglecting structural spatial information. In this work, we have implemented an anatomy assisted MAP-EM algorithm wherein the JE measure is supplied by spatial information generated using wavelet analysis. This approach has the benefit of utilizing some theoretical advantages of wavelets, including the ability to decompose an image of certain size into downsampled subbands. The proposed MAP-EM algorithm involves calculation of derivatives of the subband JE measures with respect to PET image intensities, which we have shown can be computed very similar to how inverse wavelet transform is performed. Using simulations of a mathematical human brain phantom with activities generated based on a clinical FDG study, it was observed that compared to conventional EM reconstruction, the proposed MAP-EM algorithm exhibited improved quantitative performance.**

I. INTRODUCTION

Positron emission tomography (PET) imaging continues to be affected by limited spatial resolution and inherently noisy data [1]. Techniques have been developed to improve functional PET image quality through incorporating high resolution anatomical information (e.g. MRI, CT) in the image reconstruction procedure. Mutual information (MI), or its joint entropy (JE) component, of the functional and the anatomical images have been applied by few groups [2, 3] including our own [4, 5] as *a priori* information within the Bayesian PET image reconstruction framework. Nevertheless, a potentially significant factor regarding standard MI/JE as applied to images is that spatial information is not considered; i.e. a voxel is classified merely based on its intensity information, and structural spatial information from its neighborhood is neglected.

This issue has been visited, in the image registration context, by a number of groups (e.g. see [6, 7]), including the use of local-mean or gradient feature images. An example of the application of this approach within the image reconstruction framework has also been presented in [2]. In the present work, we propose the use of a closed-form MAP-EM algorithm supplying the JE measure with spatial information generated using wavelet analysis. This approach has the benefit of utilizing some theoretical advantages of wavelets, including the ability to decompose an image of certain size into downsampled subbands, allowing concise representation of the image into individual wavelet-derived feature images, while preserving original information.

Manuscript received Nov 13, 2009.

J. Tang and A. Rahmim are with the Department of Radiology, Johns Hopkins University, Baltimore, MD 21205 (e-mails: jtang18@jhmi.edu; arahmim1@jhmi.edu).

II. METHODS

A. MAP-EM Reconstruction Algorithm

In [4], we developed a closed-form EM PET image reconstruction algorithm incorporating the JE between functional **X** and anatomical **Y** intensity images (PET and MRI in that work, and here). The anato-functional JE term $H(\mathbf{X},\mathbf{Y})$ was used as a prior within the one-step-late (OSL) MAP EM approach [8], and was calculated based on non-parametric, Parzen estimation of the probability density function, using superposition of Gaussian densities centered on samples across each image [9, 10].

The present paper extends the aforementioned work via application of JE between anato-functional feature image pairs, as derived using wavelet analysis (see Sec. II-B). For the two functional **X** and anatomical **Y** images, let us denote their k^{th} (k=1...K) wavelet generated subband feature image pair by $\{f^k(\mathbf{X}), f^k(\mathbf{Y})\}$. Instead of using the standard JE term $H(\mathbf{X},\mathbf{Y})$, the prior term in the MAP log-likelihood function was set to a weighted sum of joint entropy terms $\sum_{k=1}^{K}\beta_k H(f^k(\mathbf{X}), f^k(\mathbf{Y}))$ between each feature image pair, where β_k denotes the weighting hyperparameter for a given k^{th} wavelet subband image pair.

Thus, we sought to maximize the log-posterior probability: $\log P(\mathbf{g}\,|\,\mathbf{X}) - \sum_{k=1}^{K}\beta_k H(f^k(\mathbf{X}), f^k(\mathbf{Y}))$, where $\mathbf{g}$ is the measured data. Modeling Poisson statistics, and utilizing the OSL EM approach, we arrive at the closed-form MAP-EM algorithm:

$$x_i^{\text{new}} = \frac{x_i^{\text{old}}}{\sum_j c_{ij} + \sum_{k=1}^{K}\beta_k \frac{\partial H(f^k(\mathbf{X}), f^k(\mathbf{Y}))}{\partial x_i}\Big|_{x_i = x_i^{\text{old}}}} \sum_j \frac{c_{ij} g_j}{\sum_i c_{ij} x_i^{\text{old}}} \quad (1)$$

where g_j is the data in bin j, and c_{ij} represents an element of the system matrix modeling the contribution of voxel i to the projection bin j.

B. *Wavelet-based generation of feature images*

We propose to use the subbands generated by wavelet analysis of PET and MR image pairs as feature images, for which JEs are calculated. A 3D image can be decomposed into low frequency (L) and high frequency (H) components, via the approximation and detail wavelet filters in a particular direction. This approach can then be repeated along a second dimension, generating LL, LH, HL, HH, and finally performed along the third dimension to generate 8 image subbands (each 1/8 of total size; i.e. 1/2 size in each direction), as depicted in Fig. 1.

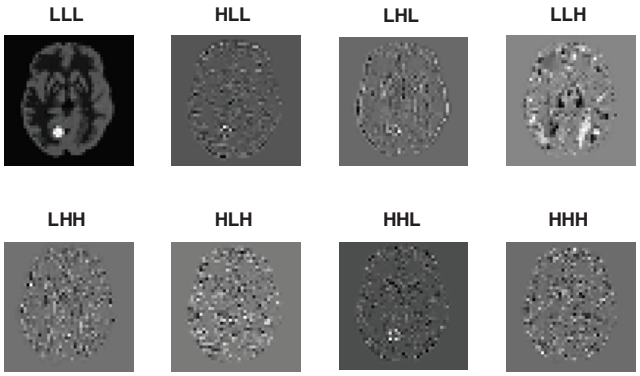

Figure 1: Transaxial slice of the 8 wavelet transform subbands of the phantom PET image, the top row from left to right shows LLL, HLL, LHL, and LLH, and the bottom row shows LHH, HLH, HHL, and HHH.

The totality of the eight subbands for each 3D image will have the same total size as the original image. It is then possible to utilize the entire information provided by all the wavelet subbands, or the most relevant portion thereof, for JE computations. In the present work, we used the nearly symmetric orthogonal wavelet bases in [11] to decompose the MR-PET image pairs. Then, as depicted in Fig. 2, we considered the JE of approximation (LLL) and first order detail (HLL, LHL, LLH) wavelet subbands, the former integrating the similarity of image intensity features, and the latter group having features comparable to gradients [12].

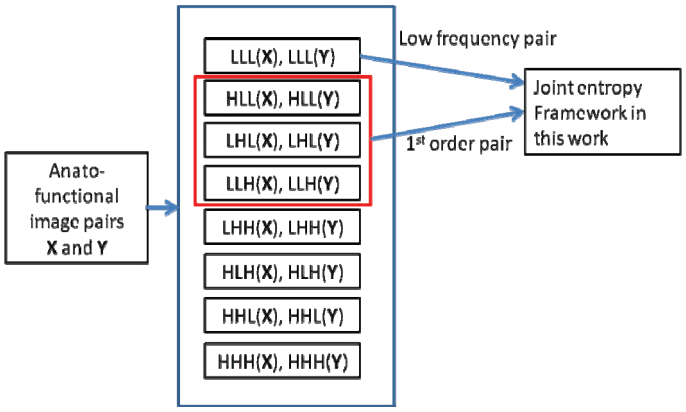

Figure 2: Joint entropy calculation scheme of wavelet subbands.

C. *Derivative of JE calculation*

Here we note that the proposed MAP-EM algorithm (1) involves calculation of the derivatives of the subband JE terms with respect to the full PET image intensities $\partial H(f^k(\mathbf{X}), f^k(\mathbf{Y}))/\partial x_i$. We are able to show that this can be performed very similar to how wavelet reconstruction (synthesis) is achieved. For simplicity, let us consider wavelet analysis along a particular dimension, and denote the wavelet subband image k by $\widehat{\mathbf{X}}^k \triangleq f^k(\mathbf{X})$ which is given by the convolution-downsampling operation:

$$\widehat{\mathbf{X}}^k = \Downarrow_2 \left\{ \mathbf{X} \otimes \mathbf{W}^k \right\} \text{ or } \hat{x}_j = \sum_u x_u w^k{}_{2j-u}, \tag{2}$$

where $\mathbf{W}^k$ is the wavelet analysis filter, and the downsampling $\Downarrow_2$ is reflected in the $2j$ index in the wavelet filter. Then, we invoke the chain rule:

$$\frac{\partial H(\widehat{\mathbf{X}}^k, \widehat{\mathbf{Y}}^k)}{\partial x_i} = \sum_l \frac{\partial H(\widehat{\mathbf{X}}^k, \widehat{\mathbf{Y}}^k)}{\partial \hat{x}_l} \frac{\partial \hat{x}_l}{\partial x_i}. \tag{3}$$

The first term may now be calculated exactly the same way as proposed in [4] using JE as applied to image intensities only, which we refer to as DSJE (derivative of standard JE). And from the definition of $\hat{x}_j$ in (2) it follows that:

$$\frac{\partial H(\widehat{\mathbf{X}}^k, \widehat{\mathbf{Y}}^k)}{\partial x_i} = \sum_l \mathrm{DSJE}_l(\widehat{\mathbf{X}}^k, \widehat{\mathbf{Y}}^k) w_{2l-i}. \tag{4}$$

Thus once the standard DSJE images are calculated, the overall derivative can be derived from a 'convolution-like' calculation. Here one may notice an interesting parallel with the wavelet reconstruction: for a synthesis filter $\overline{\mathbf{W}}^k$ defined such that $\overline{w}_m \triangleq w_{-m}$ and using the upsampling operation $\Uparrow_2$ (inserting zeros between values at odd positions), it can be shown that:

$$\frac{\partial H(\widehat{\mathbf{X}}^k, \widehat{\mathbf{Y}}^k)}{\partial x_i} = \sum_l \left[\Uparrow_2 \left\{ \mathrm{DSJE}_l(\widehat{\mathbf{X}}^k, \widehat{\mathbf{Y}}^k) \right\} \right]_l \overline{w}_{i-l}. \tag{5}$$

This now looks similar to how wavelet reconstruction is performed (i.e. upsampling each subband, followed by convolution with the synthesis filter); the only difference is that we first perform DSJE calculations on the wavelet-generated MR-PET subband pairs. Fig. 3 shows the procedure explained above for calculating the derivatives of the subband JEs with respect to the full PET image voxel intensities.

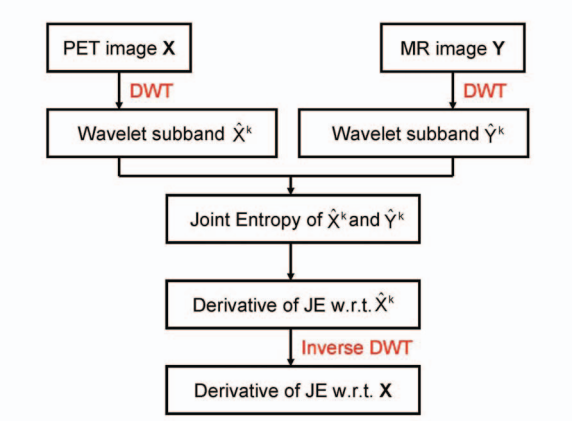

Figure 3: Diagram for calculating derivative of subband joint entropy with respect to the full PET image voxel intensities, DWT: discrete wavelet transform.

III. EXPERIMENTS AND EVALUATION

A. Phantom Simulation

We used a mathematical human brain phantom [13] for the purpose of performing realistic simulations.[1] The PET activities in the various regions of the brain were specified based on a clinical FDG study, with a corresponding MRI image generated also based on actual patient MR intensity measurements, as depicted in Fig. 4. Data were simulated for the geometry of the Discovery RX PET/CT scanner [14], except with the transaxial dimensions scaled by 0.5 to simulate a dedicated brain scanner.

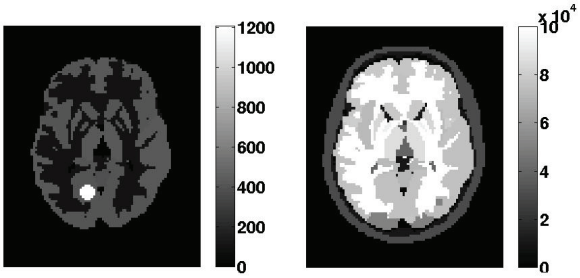

Figure 4: Transaxial slices through the human brain phantom simulating the activities of: PET (*left*) and MRI (*right*).

B. Evaluation Metrics

For each given region of interest (ROI) of known uniform intensity, as a measure of noise, the NMSE for each ROI was calculated using

$$\text{NMSE} = \left(\frac{\bar{X} - X_{true}}{X_{true}} \right)^2 , \qquad (6)$$

where $\bar{X} \triangleq \frac{1}{N} \sum_{i=1}^{N} X_i$; X_i denote the i th voxel reconstructed activity value, and N is the number of voxels in the ROI. For each ROI, the NMSE bias value was plotted against the normalized standard deviation (NSD) noise value, as calculated using

$$\text{NSD} = \frac{\sqrt{\frac{1}{N-1} \sum_{i=1}^{N} \left(X_i - \bar{X} \right)^2}}{\bar{X}} , \qquad (7)$$

where X_i and $\bar{X}$ were defined as those in (6). To quantify overall noise vs. bias performance for the entire image, we also plotted the overall NMSE versus the overall NSD. The overall NMSE is defined by averaging regional NMSE values as a measure of overall bias and the NSD values over all regions were averaged as a measure of average noise.

IV. RESULTS

For the simulated FDG study (Sec. III), Fig. 5 depicts transaxial slices through the reconstructed images from the ML-EM algorithm and the proposed MAP-EM algorithm (the 5th iterations). As shown in Fig. 2, the JEs of four subbands were incorporated in the reconstruction process. Therefore, for the two reconstructed images from above mentioned algorithms, we also display the corresponding images from wavelet analysis then wavelet synthesis with only the four subbands (LLL, HLL, LHL, and LLH). We see the improvement of the MAP-EM reconstructed image over the ML-EM reconstructed images. The same thing applies to the corresponding four-wavelet-subband recovered images.

For quantitative analysis, Fig. 6 shows the overall bias (NMSE) vs. noise (NSD) change along with iterations. It is seen that with comparable bias, the MAP-EM algorithm reduces the noise level for the reconstructed images when compared to the ML-EM algorithm. This improvement is more obvious when comparing the four-wavelet-subband recovered images, as the JEs of only those subbands were applied in the MAP-EM algorithm.

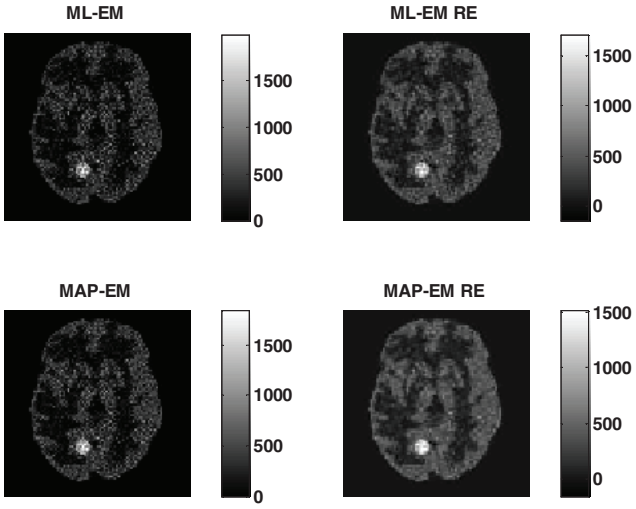

Figure 5: Transaxial slices through the reconstructed images using the ML-EM algorithm (*top left*) and the MAP-EM algorithm (*bottom left*). The corresponding four-wavelet-subband recovered images (ML-EM RE and MAP-EM RE) shown on the right.

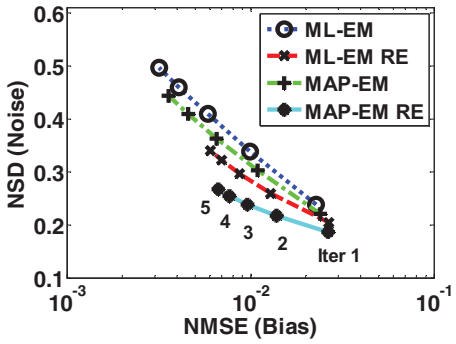

Figure 6: Overall noise (NSD) vs. bias (NMSE) plots comparing conventional ML-EM with the proposed anatomy assisted MAP-EM algorithm. Each curve were generated with increasing iterations of 1, 2, 3, 4 and 5 (21 subsets were used).

Fig. 7 shows the NSD vs. NMSE plots for a number of regions-of-interest (ROIs). As can be seen, in all the ROIs, similar to Fig. 6, the proposed technique exhibits improved quantitative performance compared to the conventional ML-EM reconstruction technique.

[1] The human brain phantom is shared for public use at: http://www.jhu.edu/rahmim/brain phantom.html

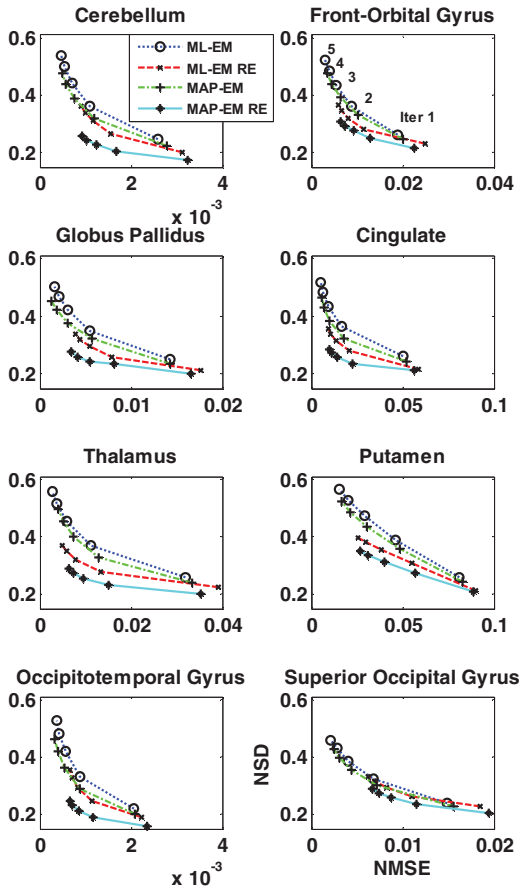

Figure 7: Regional bias (NMSE) vs. noise (NSD) for a number of ROIs, comparing conventional ML-EM algorithm with the proposed anatomy assisted MAP-EM algorithm. Each curve were generated with increasing iterations of 1, 2, 3, 4 and 5 (21 subsets were used).

V. DISCUSSION

In this work, as in [4], the covariance matrix of a given image, as used in the non-parametric Parzen window estimation of the probability distribution (in the JE measure), was assumed diagonal. The diagonal entries of a PET image, namely the variance image elements, were assumed proportional to squared voxel intensities, as motivated by previous investigations into the EM algorithm [15]. In the present work, however, such a model was only applied to the LLL subband of PET image, as other higher order feature images, corresponding to gradients, are not expected to follow such proportionality, and they were set, as in the MRI images, to obey equal variances across the images.

We found that improved performance was obtained by non-equal weighting of the feature pair image JE calculations, i.e. non-equal hyperparameters β_k as used in (1). Ongoing work includes parameter optimization for particular brain imaging tasks of interest, incorporation of an increasing number of wavelet subbands, and the study of alternative wavelet filter banks. We will then extensively evaluate whether, compared to the JE approach pursued and optimized in [4] as applied purely to image intensities, the proposed framework of utilizing wavelet-generated feature image pairs produces improved performance, given its utilization of additional spatial information.

VI. SUMMARY

We proposed to incorporate the joint entropy (JE) measure of wavelet subbands of functional and anatomical images in the PET image reconstruction so that both the voxel intensity values and the structural spatial information were taken intro account. To implement the idea, we developed an algorithm using the inverse wavelet transform scheme to relate the derivative of subband JEs to the full PET image voxel intensities. The preliminary results have demonstrated improved noise versus bias tradeoff of images reconstructed with the proposed MAP-EM algorithm compared to the conventional ML-EM algorithm. Upon further optimization of the algorithm, we will test the hypothesis that the proposed approach is able to quantitatively outperform the original JE approach, which only makes use of image intensities (and no other spatial information) within the image reconstruction framework.

ACKNOWLEDGMENT

This work was supported by the Siemens Molecular Imaging grant JHU-MR-33-01. The authors wish to thank Andrew Crabb for computational support.

REFERENCES

[1] A. Rahmim and H. Zaidi, "PET versus SPECT: strengths, limitations and challenges," *Nucl Med Commun,* vol. 29, pp. 193-207, Mar 2008.

[2] S. Somayajula, E. Asma, and R. M. Leahy, "PET image reconstruction using anatomical information through mutual information based priors," *IEEE Nucl. Sci. Symp. Conference Record,* vol. 5, pp. 2722-26, 2005.

[3] J. Nuyts, "The use of mutual information and joint entropy for anatomical priors in emission tomography," *IEEE Nucl. Sci. Symp. Conference Record,* vol. 6, pp. 4149-54, 2007.

[4] J. Tang and A. Rahmim, "Bayesian PET image reconstruction incorporating anato-functional joint entropy," *Phys. Med. Bio.,* vol. 54, pp. 7063-7075, 2009.

[5] J. Tang, H. Kuwabara, D. F. Wong, and A. Rahmim, "Direct 4D reconstruction of parametric images incorporating anato-functional joint entropy," *IEEE Nucl. Sci. Symp. Conf. Record,* pp. 5471-5474, 2008.

[6] D. B. Russakoff, C. Tomasi, R. T., and M. C. R., "Image similarity using mutual information of regions," in *8th Europ. Conf. on Computer Vision (ECCV)*. vol. LNCS 3023, T. Pajdla and J. Matas, Eds., 2004, pp. 596-607.

[7] J. P. W. Pluim, J. B. A. Maintz, and M. A. Viergever, "Image registration by maximization of combined mutual information and gradient information," *Medical Imaging, IEEE Transactions on,* vol. 19, pp. 809-814, 2000.

[8] P. J. Green, "Bayesian reconstructions from emission tomography data using a modified EM algorithm.," *IEEE Trans Med Imaging,* vol. 9, pp. 84-93, 1990.

[9] P. A. Viola, "Alignment by maximization of mutual information (PhD thesis)." vol. PhD: Massachusetts Institute of Technology, 1995.

[10] R. O. Duda, P. E. Hart, and D. G. Stork, *Pattern classification*, Second ed.: Wiley, 2001.

[11] A. F. Abdelnour and I. W. Selesnick, "Nearly symmetric orthogonal wavelet bases," in *IEEE Intern. Conf. Acoust., Speech, Signal Processing (ICASSP)*, 2001.

[12] R. Xu and Y.-W. Chen, "Wavelet-based multiresolution medical image registration strategy combining mutual information with spatial information," *Intern. Journ. Innov. Comput. Inform. Control (ICIC),* vol. 3, pp. 285-296, 2007.

[13] A. Rahmim, K. Dinelle, J. C. Cheng, M. A. Shilov, W. P. Segars, S. C. Lidstone, S. Blinder, O. G. Rousset, H. Vajihollahi, B. M. Tsui, D. F. Wong, and V. Sossi, "Accurate event-driven motion compensation in high-resolution PET incorporating scattered and random events," *IEEE Trans Med Imaging,* vol. 27, pp. 1018-33, Aug 2008.

[14] B. J. Kemp, C. Kim, J. J. Williams, A. Ganin, and V. J. Lowe, "NEMA NU 2-2001 performance measurements of an LYSO-based PET/CT system in 2D and 3D acquisition modes," *J Nucl Med,* vol. 47, pp. 1960-7, Dec 2006.

[15] H. H. Barrett, D. W. Wilson, and B. M. W. Tsui, "Noise properties of the EM algorithm. I. Theory.," *Phys Med Biol,* vol. 39, pp. 833-846, 1994.